THE JOURNAL OF PHYSICAL CHEMISTRY B
A JOURNAL OF THE AMERICAN CHEMICAL SOCIETY

pubs.acs.org/JPCB

Article

Molecular Dynamics and Experimental Study of the Effect of CeF_3 and NdF_3 Additives on the Physical Properties of FLiNaK

A. Y. Galashev,* O. R. Rakhmanova, K. A. Abramova, K. P. Katin, M. M. Maslov, O. Y. Tkacheva, A. V. Rudenko, A. A. Kataev, and Y. P. Zaikov

Cite This: *J. Phys. Chem. B* 2023, 127, 1197−1208

Read Online

ACCESS | Metrics & More | Article Recommendations | Supporting Information

ABSTRACT: The paper presents the results, which are consistent within 2%, obtained both in the simulation of molecular dynamics and in the experiment on the study of the kinetic properties of molten FLiNaK with addition of lanthanide fluorides. The parameters of the Born−Huggins−Meier potential for the interaction of CeF_3 or NdF_3 with FLiNaK components are first calculated using the ab initio approach. The enthalpy of the system with dissolved CeF_3 or NdF_3 calculated in the model increases by ∼4.4% over the entire temperature range studied ($800 \le T \le 1020$ K). The self-diffusion coefficients of the molten salt components are calculated from the Einstein relation and also estimated from the shear viscosity data. The temperature dependences of the shear viscosity of molten FLiNaK as well as FLiNaK with additions of 15 mol % CeF_3 or NdF_3 are determined experimentally and by calculation. In addition, the dependence of shear viscosity on the concentration of CeF_3 and NdF_3 in FLiNaK is measured and calculated. The linear growth of the shear viscosity with the CeF_3 and NdF_3 concentrations is obtained. Experimental dependence is in good agreement with the simulated results in the case of NdF_3, and there is the discrepancy while CeF_3 addition. An analytical approximation of the temperature and concentration dependences for the viscosity of molten FliNaK and for the calculated self-diffusion coefficients of constituent elements is proposed. Linear approximation of temperature dependence of the self-diffusion coefficients of similar components in the corresponding extended systems is presented.

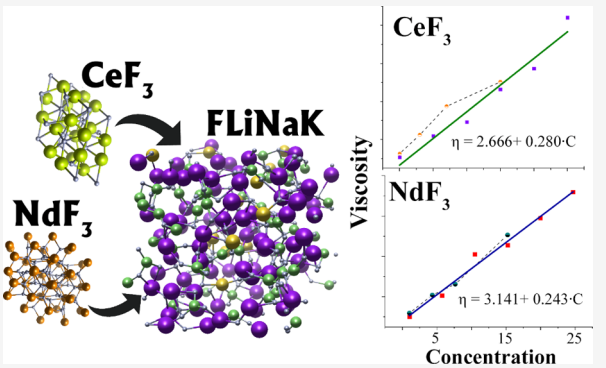

INTRODUCTION

The concept of a molten salt reactor (MSR) got its start in the 1960s, but the industrial technology has not been realized yet. Currently, the problem of radioactive waste management is acute, and one of the promising solutions is the use of MSR as a breeder for the transmutation of minor actinides.[1−3] Recently, MSRs have been developed, in which chloride and fluoride salts are used not only as coolants but also as liquid fuels.[4] In this case, the molten salt used as fuel contains thorium and uranium. With the rapid multiplication of neutrons, the MSR may contain no Th at all. Rapid MSRs based on the chloride salt serve a different purpose. By producing large quantities of fast neutrons, they are used as nuclear waste incinerators. A negative temperature reactivity gradient, low pressure, and no chemical reaction with air or water make these reactors safer to operate compared to conventional solid-state reactors. The main problem of the manufactured MSR is the possible leakage of fission products and reactive products that can corrode the containment.

According to the authors of works[4,5] who reviewed the concepts of nuclear reactors, in which the use of molten salts is assumed, the fluoride salts are the most advanced among salt mixtures for MSRs. On one hand, fluoride salts, when heated, have an atmospheric boiling point above 1273 K. They are used at high operating temperatures and are highly corrosive.[6] But on the other hand, they are stable for irradiation and have minimal parasitic neutron absorption. Molten fluorides can be used as fuel, coolants, and solvents in molten salt reactors.[4]

MSR fuel consists of a carrier, which is a mixture of molten fluoride salts, and dissolved in this mixture fissile material. The content of fission products increases during reactor operation, and mostly, it refers to neutron poisons, which should be removed from the melt.

Requirements for molten mixtures used as a fuel salt have been summarized in the papers:[7,8] a low neutron capture cross-section, a low melting temperature, which ensures the operating temperature of the reactor of 770−970 K, low corrosivity, a high heat capacity and electrical conductivity, and a low viscosity. The cooling salt must be stable and compatible

Received: September 29, 2022
Revised: January 11, 2023
Published: January 25, 2023

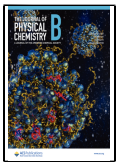

https://doi.org/10.1021/acs.jpcb.2c06915
J. Phys. Chem. B 2023, 127, 1197−1208

with the structural material of the heat exchangers, have good heat-transfer and hydrodynamic properties, and have a low vapor pressure over a wide operating range.

Mixtures of alkali and alkaline earth metal fluorides, such as LiF−BeF_2 (FLiBe) and LiF−NaF−KF (FLiNaK), are predominantly considered as carrier salts. Their physicochemical properties have been extensively studied at Oak Ridge National Laboratory for the use in MSR.[9] Both melts have a fairly low liquidus temperature and suitable thermophysical properties. However, mixtures of beryllium require special and costly handling efforts due to their toxicity. For this reason, FLiNaK has become the main alternative to FLiBe in some cases due to its low toxicity and the heat-transfer and chemical properties similar to those of FLiBe. The molten eutectic FLiNaK has another advantage, that is, the high solubility of fissile materials, which is the most important criterion for choosing a salt solvent.

There is a significant temperature margin for using FLiNaK as a coolant. Its boiling point is ∼500 K above the maximal peak coolant temperatures. The thermophysical properties of molten fluoride salts are still not well understood. That leads to significant uncertainties and makes it difficult to design and operate the nuclear facility using FLiNaK. Uncertainty from the selection of coolant properties can be included in the simulation to get a complete picture of the cooling process. There are a number of works devoted to the investigation of the molten salts.[10−16]

It should be taken into account that high concentrations of actinide fluorides can significantly impact the physicochemical properties of solvent melts. However, the study of this effect requires rather complex equipment, time, and material costs.[17] It is much more efficient to carry out the necessary investigations by applying the analogues of actinides—lanthanides, which are close in physicochemical, thermodynamic, and crystallographic properties. It is known[17,18] that lanthanide fluorides CeF_3 and NdF_3 are imitators of actinide fluorides PuF_3 and AmF_3, correspondently.

For most of the salts used in the reactor, the shear viscosity follows an Arrhenius behavior over the range of possible operating temperatures. In other words, the molten salts are Newtonian fluids that exhibit a typical exponential decrease in viscosity with increasing temperature. However, the decomposition of some salts at high temperatures or prolonged exposure to heat leads to the fact that the temperature dependence of viscosity ceases to obey the Arrhenius law.[19] Even though there is a significant database, there are a number of important mixtures for which no viscosity information exists. The molten FLiNaK with CeF_3 and NdF_3 is among such mixtures.

There are quite a lot of experimental data on the FLiNaK viscosity in a wide temperature range.[20−24] In contrast, the literature contains a rather limited number of works regarding the viscosity of the FLiNaK−CeF_3 molten system.[25] Moreover, the behavior of viscosity with a change in the CeF_3 concentration found in Ref 25 turned out to be unpredictable. Thus, it was found that the addition of 5 mol % CeF_3 to the molten FLiNaK reduces the kinematic viscosity at temperatures of 750−820 K and somewhat increases it in the range of 820−1200 K, while the addition of 10 mol % CeF_3 does not give the same effect. The viscosity data for the FLiNaK−NdF_3 system were not found in the literature. The physical properties of multicomponent salts are determined with a large error. For example, data on thermal diffusivity are of the order of relative uncertainties of 10−15%.[26]

The main goal of this work is to study the kinetic properties of the eutectic mixture (46.5−11.5−42.0 mol %) of LiF−NaF−KF as well as FLiNaK containing cerium and neodymium fluorides in a temperature range covering the operating temperatures of MSR and at concentrations of additions (including actinides) corresponding to that of the molten salt in the reactor. We assume that the lanthanide fluorides CeF_3 and NdF_3 in the FLiNaK molten salt can serve as imitators of the actinide fluorides PuF_3 and AmF_3, respectively. To solve the problem, we use both experiments and molecular dynamics (MD) calculations.

METHODS

Creation of Interatomic Interaction Potentials. Born−Huggins−Mayer potential[27] is used to simulate the interatomic interactions in molten FLiNaK system (see the Supporting Information for the potential description and parameters). The parameters of the non-Coulomb core−core ionic repulsions between Ce^{3+} and others ions were fitted based on the results of the density functional theory (DFT) calculations. For cerium−fluorine interactions, we considered the flat CeF_3 molecule, in which the cerium atom is placed in the center of a regular triangle formed by three fluorine atoms (see Figure 1a). We varied the Ce−F distance r_1 keeping unchanged the symmetry of the system. The total molecule energy U_{DFT} was considered as a sum of Coulomb U_C and non-Coulomb U_{NC}

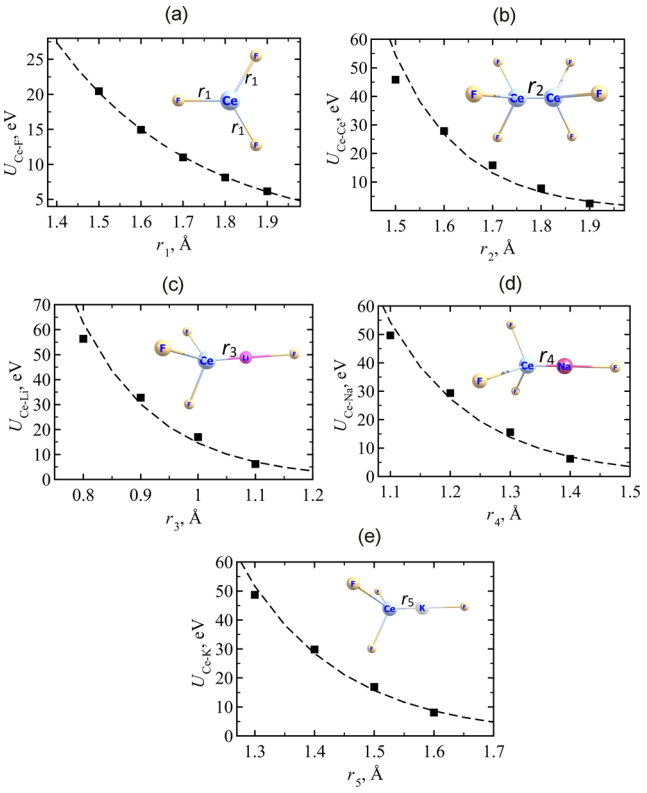

Figure 1. Non-Coulomb contribution to the interaction of Ce^{3+} ion with F^- (a), Ce^{3+} (b), Li^+(c), Na^+, (d) and K^+ (e) ions. Black squares are results of DFT calculations; dashed lines are exponential fittings (see formulas 2 and 3). The insets show the model electroneutral systems used for calculations. In (b−e), all distances between metal and fluorine atoms are equal to 2.3 Å.

https://doi.org/10.1021/acs.jpcb.2c06915
J. Phys. Chem. B 2023, 127, 1197−1208

Table 1. Fitted Parameters for Interaction of Ce^{3+} and Nd^{3+} with the Components of FLiNaK

cerium	B, eV	ρ, Å	σ, Å	neodymium	B, eV	ρ, Å	σ, Å
$Ce^{3+}-Ce^{3+}$	1.357	0.141	2.02	$Nd^{3+}-Nd^{3+}$	0.723	0.117	1.96
$Ce^{3+}-F^-$	1.618	0.3324	2.34	$Nd^{3+}-F^-$	1.634	0.3328	2.31
$Ce^{3+}-Li^+$	0.053	0.137	1.77	$Nd^{3+}-Li^+$	0.012	0.110	1.74
$Ce^{3+}-Na^+$	0.092	0.146	2.03	$Nd^{3+}-Na^+$	0.028	0.121	2.00
$Ce^{3+}-K^+$	0.078	0.168	2.39	$Nd^{3+}-K^+$	0.032	0.146	2.36

contributions. The value of U_C was calculated as the pair electrostatic energy of point charges ($-|e|$ for fluorine atoms and $+3|e|$ for cerium atom, where e is the elementary charge). The U_{NC} value was calculated as a difference between total energy U_{DFT} and Coulomb term U_C. The Ce−F non-Coulomb interaction energy U_{Ce-F} was evaluated from DFT results as

$$U_{Ce-F}(r_1) = (U_{NC}(r_1) - U_{NC}(5\ \text{Å}))/3 \quad (1)$$

Here, we assume that non-Coulomb interactions are negligible at r = 5 Å and can be used as a reference point; denominator 3 is due to three equivalent fluorine atoms. Calculated energies $U_{Ce-F}(r_1)$ at different values of r_1 were fitted with the selected exponential empirical curve

$$U_{Ce-F}(r_1) \approx B\ \exp((\sigma_1 - r_1)/\rho) \quad (2)$$

In this formula, σ_1 = 2.34 Å is a sum of ionic radii of Ce^{3+} and F^- ions (1.01 and 1.33 Å, respectively); parameters B and ρ are fitted according to the least square error method, see Figure 1a. Obtained values of B and ρ are listed in Table 1.

To probe the cerium−cerium interaction into the melting salt, we considered a more complex model system consisting of two cerium and six fluorine atoms, see Figure 1b. In this system, all Ce−F distances are fixed and equal to 2.3 Å (typical value for the melting salts), whereas Ce−Ce distance r_2 was varied. The total interaction energy between two CeF_3 was calculated as $U_{(Ce_2F_6)} - 2U_{(CeF_3)}$. Similar to the case described above, this energy was divided into Coulomb and non-Coulomb contributions. We assume that the obtained non-Coulomb interaction between two CeF_3 is only due to Ce−Ce interactions. Therefore, obtained from DFT, Ce−Ce non-Coulomb interaction energy was fitted with the same empirical dependence

$$U_{Ce-Ce}(r_2) \approx B\ \exp((\sigma_2 - r_2)/\rho) \quad (3)$$

Here, σ_1 = 2.02 Å is the double ionic radius of Ce^{3+} ion. The results of fitting are presented in Figure 1b and Table 1.

For interactions of Ce^{3+} with the alkali metals ions X (X = Li^+, Na^+, K^+), we regarded the interaction between CeF_3 and XF complexes as presented in Figure 1c−e. In these systems, the Ce−F and X−F distances are also fixed and equal to 2.3 Å, whereas Ce−X distances (r_3, r_4, and r_5) were varied. For these models, the DFT interaction energy between CeF_3 and XF was computed as $U_{(CeF_3XF)} - U_{(CeF_3)} - U_{(XF)}$. Similar to the previous case, the non-Coulomb part of this interaction energy was assumed to appear due to the Ce−X non-Coulomb interactions. These interactions were fitted with the formulas similar to (2) and (3). The results are shown in Figure 1c−e and Table 1.

All the calculations performed for Ce^{3+} ion were repeated for neodymium ion Nd^{3+}. The values of fitted parameters are also listed in Table 1.

DFT energies of considered systems were computed with the QUANTUM ESPRESSO program.[28,29] We used projector-augmented wave GGA-PBE scalar relativistic pseudopotentials[30,31] with the kinetic energy cutoff for wave functions and a charge density of 100 and 400 Ry, respectively. All systems were placed in a simple cubic lattice with the large parameter a = 30 Å. Therefore, any interaction between periodic cells was negligible. Since we in fact have dealt with non-periodic isolated systems, the only Γ-points in the k-spaces were considered. Grimme's dispersion corrections D3 were added for accurate accounting of non-covalent interactions.[32]

MD Model: Simulation of the Molten FLiNaK System. The MD model of pure FLiNaK corresponds to its eutectic composition: 46.5 mol % LiF, 11.5 mol % NaF, and 42.0 mol % KF.[33] At atmospheric pressure, the experimental melting and boiling points for this eutectic fluoride system are 727 and 1843 K, respectively. The melt is formed by melting the LiF, NaF, and KF crystals. The crystals have the face-centered cubic lattice with lattice parameters of a = 0.40279 nm for LiF, a = 0.46344 nm for NaF, and a = 0.534 nm for KF.[34] The crystals are located in the rectangular cell with sizes of $x \times y \times z$: 12.1 × 3.4 × 11.7 nm. The total number of ions in the system is 20,000. The number of ions of each type corresponds to the eutectic composition of FLiNaK. Before the start of the main simulation, the geometric optimization of the system is executed.

The first stage runs were performed in canonical ensemble (NVT) where the gradual system heating up to 3000 K during 2,500,000 time steps (2.5 ns) was executed for melting crystals and reaching the finest melt mixing. The second stage runs lasted during 1,000,000 time steps (1 ns) for cooling the system up to a desirable temperature from the range of $750 \le T \le 1020$ K (15 values) in the isothermal−isobaric ensemble (NPT). Then, after relaxation of the system during 0.5 ns, the shear viscosity using Green−Kubo method was calculated during 1 ns in the micro-canonical ensemble (NVE). The Nose−Hoover thermostat and barostat[35,36] were used for keeping constant the simulated temperature and pressure, respectively.

The periodic boundary conditions were used for all calculations. Long-range interactions were handled using the PPPM (a particle−particle particle−mesh) summation method,[37] where the solver maps atom charges to a 3D mesh and uses 3D fastest Fourier transform to solve Poisson's equation on the mesh and then interpolates electric fields on the mesh points back to the charged particles. Comparing with the traditional Ewald summation,[38] where the cost scales as $N^{3/2}$ (N is the number of atoms in the system), PPPM solver (due to Fourier transform) scales as $N \log N$, which is almost always a faster choice.[39] Verlet algorithm[40] was used to solve Newton's equations of motion with a time step of $\Delta t = 10^{-15}$ s.

MD Model: Simulation of the FLiNaK + CeF_3 and FLiNaK + NdF_3 Systems. To form the molten system FLiNaK containing additives of lanthanide fluorides (Ce or Nd), at the time moment t = 0, the crystal CeF_3 or NdF_3 is

https://doi.org/10.1021/acs.jpcb.2c06915
J. Phys. Chem. B 2023, 127, 1197−1208

added to the LiF, NaF, and KF crystals which are in the composition corresponding to the eutectic one in the obtaining melt. The lattice parameters for the lanthanide fluorides are[41] a = 0.7120 nm, c = 0.7273 nm for CeF_3 and a = 0.7018 nm, c = 0.7187 nm for NdF_3. The CeF_3 and NdF_3 crystals have the trigonal crystal structure with the $P3c1$ space group. As a result, the molten system has the necessary concentration of the lanthanide fluoride: 5, 10, 15, 20, or 25 mol %. It is an experimental fact that the solubility of CeF_3 and NdF_3 in LiF−NaF−KF molten system can reach up to 40 mol % in the temperature range of 823−1073 K.[19] Then, all the stages of the systems melting and equilibrating (in *NVT* ensemble) and property calculations (in *NPT* and *NVE* ensembles) are repeated as for the pure FLiNaK calculations. The general view of the FLiNaK + 15 mol % CeF_3 system corresponding to the time moment t = 0 s (left picture) as well as the totally molten, mixed, and equilibrated system obtained by the time moment t = 2.5 ns (right picture) is shown in Figure 2.

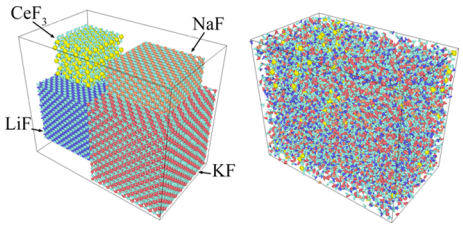

Figure 2. General view of the FLiNaK + 15 mol % CeF_3 system before the MD run (t = 0 s, left picture) and after, when the overheated melt received at T = 3000 K (t = 2.5 ns, right picture).

The working concentration of all additions (minor actinides fluorides) in FLiNaK is up to 10−15 mol % at T = 975 K.[1] It is believed to be higher at T = 1023 K. However, it is impossible in the experiment to make a difference between the properties when the addition concentrations are less than 5 mol %.[18] We study the temperature dependence of the physicochemical properties of these molten salts at the maximum CeF_3 or NdF_3 concentration (15%) achieved under industrial conditions. However, while studying the concentration dependence of the shear viscosity with MD, the upper limit of the concentration of these additions was extended.

More precisely, for the FLiNaK + CeF_3 and FLiNaK + NdF_3 systems, two sets of calculations are executed. In the first set, at a constant concentration of CeF_3 or NdF_3 additives (15 mol %), the system properties are calculated for the following temperatures: 800, 820, 840, 850, 875, 900, 950, 975, 1000, and 1020 K. In the second set, at a constant temperature of T = 975 K (corresponding to the operation temperature of MSR[42]), the concentration of the lanthanide fluorides additives varies as follows: 5, 10, 15, 20, and 25 mol %. Table 2 presents the total number of ions in every system depending on the lanthanide fluoride concentration.

The comparison of the molten systems properties evaluated in the present calculations with the experimental and other simulated data makes it possible to estimate the degree of reliability of the designed model. Figure 3 shows the temperature dependence of the internal energy of the pure FLiNaK and FLiNaK + 15 mol % CeF_3 systems. The transition of the system from the crystal to the molten state can be vividly seen in the temperature range of 680−760 K (pure FLiNaK) and 770−860 K (FLiNaK + 15 mol % CeF_3). According to the experimental data,[4] the eutectic point of the pure FLiNaK

Table 2. Number of Ions of Each Type in the Systems under Consideration

mole fraction of lanthanide fluoride in the system (%)	types of ions forming the systems					
	Li^+	Na^+	K^+	F^-	Ce^{3+}	Nd^{3+}
0	4650	1150	4200	10,000	0	0
5	4650	1150	4200	10,750	250	250
10	4650	1150	4200	11,500	500	500
15	4650	1150	4200	12,250	750	750
20	4650	1150	4200	13,000	1000	1000
25	4650	1150	4200	13,750	1250	1250

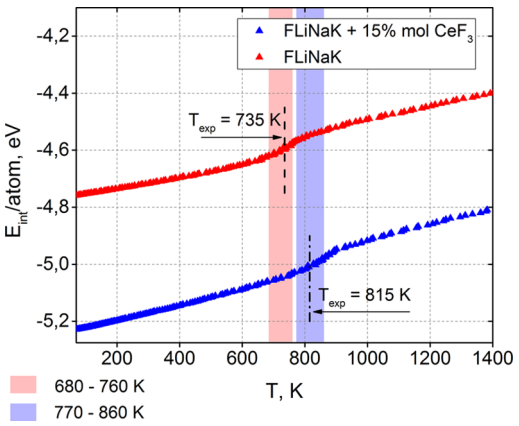

Figure 3. Temperature dependence of the internal energy E_{int} for the FLiNaK system (red curve) and FLiNaK + 15 mol % CeF_3 system (blue curve); the vertical color bands highlight the inflection areas where the transition of the system from the solid to the liquid state occurs; the vertical dash lines show the experimental values of liquidus for FLiNaK[4] and FLiNaK + 15 mol % CeF_3 systems.[43]

system locates at T = 735 K. The addition of 15 mol % CeF_3 to FLiNaK shifts the liquidus point to the area of higher temperatures to the value of T = 815 K.[43]

Calculation of the Self-Diffusion Coefficient of the FLiNaK Components. Mass transfer in the molten salts largely determines the kinetics of the electrode processes and influences significantly the selection of the optimal electrolysis conditions. However, the measurement of the self-diffusion coefficient D in the molten salts often encounters many difficulties.[44] Electrochemical methods for measuring D are the fastest and do not require any special tools. These methods are based on the quantitative analysis of the electrochemical response during mass transfer. As a rule, the implementation of the electrochemical method requires knowledge of the number of electrons involved in the electrode reaction and determination of the electrode area and the volume concentration of particles carrying an electric charge. The determination of these characteristics is not a trivial task and often leads to significant errors in the measurement of D. In this regard, it is very important to calculate the self-diffusion coefficients for the components of the molten salt using the MD method.

The mean square displacement (MSD) $\langle \Delta r^2 \rangle$ of the center of mass of similar atoms is defined as

https://doi.org/10.1021/acs.jpcb.2c06915
J. Phys. Chem. B 2023, 127, 1197−1208

$$\langle \Delta r^2 \rangle = \left\langle \frac{1}{N}\sum_{i=0}^{N} [r_i(t_0 + \mathrm{d}t) - r_i(t_0)]^2 \right\rangle = \frac{1}{N \cdot n_t}\sum_{i=0}^{N}\sum_{j=0}^{n_t} [r_i(t_j + \mathrm{d}t) - r_i(t_j)]^2 \quad (4)$$

where N is the number of atoms of a certain sort, n_t is the number of intervals for determining $\langle \Delta r^2 \rangle$, and t_0 and t_j are the initial time moments.

The coefficient D is determined from the slope of the $\langle \Delta r^2 \rangle$ dependence on time. Thus, the self-diffusion coefficient D of atoms is calculated from the Einstein relation

$$D = \frac{1}{6}\lim_{t\to\infty} \langle \Delta r^2 \rangle / t \quad (5)$$

In our model, the self-diffusion coefficients are calculated in the *NPT* ensemble. The jumps of atoms in the *NPT* ensemble increase compared to jumps in the *NVT* one. That leads to the higher self-diffusion coefficients in the ensemble with constant pressure.[45] It is a frequent case, when the self-diffusion coefficients calculated according to eq 5 exceed the experimental values. Another reason could be the short monitoring time of the system lifecycle in the MD simulation. Two transport modes can be distinguished in a liquid as ballistic and diffusion.[46] The first collisionless mode is observed at the earlier simulation times. The second mode is represented as the random wanderings. It is based on the molecule collisions and expressed as the linear dependence of the mean square displacements on time. For liquids with low diffusivity, the nonlinearity of $\langle \Delta r^2 \rangle(t)$ function keeps saving longer than that for the liquids with high diffusivity. For the determination of D coefficient, we do not take into account the nonlinear initial segment of the $\langle \Delta r^2 \rangle(t)$ dependence. As a result of the short monitoring time of the system lifecycle, the selected linear segments of this dependence (used for D coefficient determination) could be still influenced by ballistic mode. Finally, it disappears at the infinite times out of simulation. This effect gives the overestimated self-diffusion coefficient.

In ref 47, based on the hydrodynamic model of a particle surrounded by a solvent, an analytical correction was obtained to the effect of the system size on the diffusion coefficient. In this approach, it was assumed that particle diffusion depends not only on the hydrodynamic interaction with the solvent in the nearest environment but also on periodic images of the particle itself and the solvent. An expression was obtained for the self-diffusion coefficient D_∞ of the particle in an infinite system

$$D_\infty = D_{\mathrm{PBC}}^{\mathrm{MD}} + \frac{k_\mathrm{B} T \xi}{6\pi\eta L} \quad (6)$$

where $D_{\mathrm{PBC}}^{\mathrm{MD}}$ is the self-diffusion coefficient obtained in the MD model with periodic boundary conditions (PBCs), k_B is the Boltzmann constant, T is the temperature, η is the shear viscosity, L is an effective length of the simulation cell, and constant $\xi = 2.837297$.[48] In the case of unequal lengths of edges in a cubic cell, we can set $L = \overline{L}$, where $\overline{L}$ is the average length of the cell edge.

The hydrodynamic radius R_h can be calculated from the Stokes−Einstein correlation between the self-diffusion coefficient and the shear viscosity[49]

$$R_\mathrm{h} = \frac{k_\mathrm{B} T}{6\pi\eta D} \quad (7)$$

This radius calculated from the diffusion properties of the particle is indicative of the apparent size of the dynamic hydrated/solvated particle. If we assume that the ion in the melt moves completely separately from the environment, then we can assume that the hydrodynamic radius is equal to the radius of the ion. In this approximation, the self-diffusion coefficient D_η of unbound ions can be estimated as

$$D_\eta = \frac{kT}{6\pi\eta R_i} \quad (8)$$

where R_i is the ion radius.

Shear Viscosity in the Model. The shear viscosity η is a measure of the resistance of a fluid to being deformed by shear stress. MD simulations can be used to predict viscosity using either equilibrium or none equilibrium methods. In the present work, the viscosity is calculated on the basis of Green−Kubo equation[50] using the time integral of the off-diagonal stress tensor auto-correlation function in a totally equilibrated system

$$\eta = \frac{1}{k_\mathrm{B} T V}\int_0^\infty \langle S_{xy}(0) S_{xy}(t) \rangle \mathrm{d}t \quad (9)$$

where V is the simulation cell volume and S_{xy} is the xy-component of the stress tensor, which is defined as follows

$$S_{xy} = \sum_{i=1}^{N}\left[m_i v_{xi} v_{yi} + \frac{1}{2}\sum_{j\neq i} x_{ij} f_y(r_{ij}) \right] \quad (10)$$

where m_i is the mass of ion i, v_{xi} and v_{yi} are the x- and y-components of the v_i velocity of ion i, respectively, x_{ij} is the x-component corresponding to the distance $r_{ij} = r_i - r_j$, and $f_y(r_{ij})$ is the y-component of the force on ion i due to ion j. Each of three independent off-diagonal components of the stress tensor (S_{xj}, S_{xz}, and S_{yz}) provides an independent estimate of shear viscosity, and the averaged value is taken as the final viscosity value.[51]

All calculations were performed with the use of the open source program code for MD simulation LAMMPS[52] on a URAN cluster-type hybrid computer at the N. N. Krasovskii Institute of Mathematics and Mechanics UB RAS with a peak performance of 216 Tflop/s and 1864 CPUs.

Experimental: Chemicals. Lithium fluoride LiF (mass fraction of LiF 99.0%) (CJSC VECTON), sodium fluoride NaF (mass fraction of NaF 99.0%) (LLC "GRANCHIM"), and potassium fluoride acidic KF·HF (mass fraction of KF·HF 99−101%) (LLC "GRANCHIM") were used for the preparation of the 46.5LiF−11.5NaF−42KF (mol %) eutectic mixture. KF·HF decomposes at 673−773 K; the released HF prevents the hydrolysis of salts and simultaneously fluorinates oxygen-containing impurities. The preparation technique is described in detail in our previous work.[53]

The neodymium and cerium trifluorides were prepared by hydrofluorination of Nd_2O_3 and CeO_2 oxides according to the technique described in our previous work.[53] X-ray fluorescence analysis (Rigaku MiniFlex 600) of the obtained samples confirms the presence of NdF_3 and CeF_3 phases only, correspondently.

The viscosity of FLiNaK melts with NdF_3 or CeF_3 up to 15 mol % was measured in the temperature range from liquidus to 1073 K.

https://doi.org/10.1021/acs.jpcb.2c06915
J. Phys. Chem. B 2023, 127, 1197−1208

Experimental: Rotational Viscometry Method. The shear viscosity of the melts is determined with the use of a high-temperature rotary rheometer FRS-1600 (Anton Paar, Austria) with the international standard of ISO 7884-2. The investigated melt is located between two graphite cylinders in a small gap (2 mm). The outer cylinder (outer height 150 mm, inner height 60 mm, outer diameter 40 mm, and inner diameter 30 mm) is stationary, while the inner cylinder (rotor) (height 20 mm and diameter 15 mm) rotates at a constant speed. The rotor is immersed in the melt to a depth of 12 mm from the bottom of the crucible. The viscosity is measured in an inert gas atmosphere.

The area of laminar motion of the melt is determined from the viscosity curves at a constant temperature, and the shear rate parameter at which the viscosity does not depend on the shear rate is chosen. The temperature dependence of viscosity is obtained at a constant shear rate of 12 s^{-1} according to a given melt cooling program of 2 °/min. The procedure for measuring the viscosity of fluoride melts is described in detail in our previous work.[54]

RESULTS AND DISCUSSION

Recently, a semi-quantitative description of some properties of molten FLiNaK was accomplished in ref 55. In this work, a truncated interaction potential that does not contain dispersion terms was used. However, to improve the Born−Meier potential, the author used the parameters fitted to the ab initio data on the energies of ion pairs. The densities of molten FLiNaK obtained in ref 55 turned out to be 4−5% lower than that obtained in experiments in the temperature range of 750−1000 K. The ion self-diffusion coefficients calculated in ref 55 were noticeably lower than the experimental values,[56] especially for F^- and Li^+ ions, and the thermal conductivity of FLiNaK in the considered temperature range was significantly higher than the experimental values.[57] The dispersion energy of the systems with Coulomb interactions can be up to 10% of the total energy of the system.[58] The neglect of dispersion forces in the interionic interaction, first of all, strongly affects the accuracy of reproducing the kinetic properties of the system.

The present study takes into account the dispersion interaction, and we do not fit the parameters of the Born−Meyer potential, as was done in ref 55. We calculate the physical properties of molten FLiNak over almost the same temperature range. Among these properties are the density of the melt, the ion self-diffusion coefficients, and the shear viscosity. With the closeness of the calculated properties to the corresponding experimental characteristics, one can judge whether the interaction potentials used are adequate.

The temperature dependence of the simulated and experimental densities of molten FLiNaK is shown in Figure 4. Our calculated densities differ from the corresponding model data of Salanne et al.[60] (obtained with allowance for the polarizing effect) by no more than 3.4% and from the experimental data[59] by less than 1.2%. The density of the FLiNaK + 15 mol % CeF_3 system determined by us at T = 975 K is 2.56091 g/cm^3, while the experimental density at this temperature is 2.56179 g/cm^3.

The partial radial distribution functions (RDFs) for Li−F, Na−F, and K−F corresponding to the temperature of T = 1000 K (solid lines) in the comparison with the RDF obtained in ab initio calculations (the system consists of 100 ions at T = 973 K)[56] (dashed lines) are shown in Figure 5. There is good agreement of the locations of RDF maxima between our calculations and functions from work.[56]

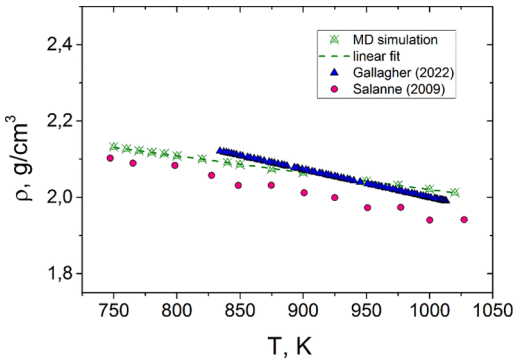

Figure 4. Simulated and experimental densities of molten FLiNaK; the dashed line shows the linear fit of our MD data; blue triangles present the results of the experiment;[59] pink dots give the simulated data obtained in the polarizable MD model.[60]

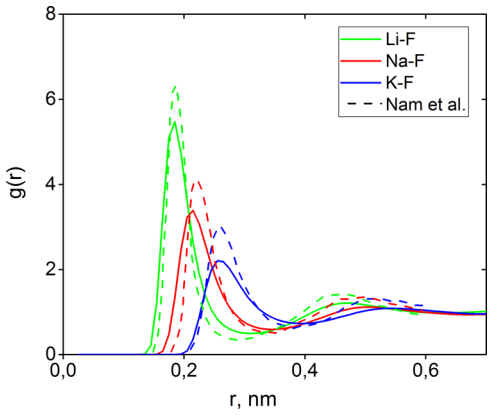

Figure 5. Partial RDFs of pure FLiNaK at a temperature of 1000 K (solid lines); RDF obtained in the ab initio calculation[56] (dashed lines) at T = 973 K.

The thermal effect of a process taking place at constant pressure is expressed in terms of enthalpy H. The quantitates of value H obtained in our MD calculation for pure FLiNaK differ from the higher values of work,[60] no more than 2.2% (Figure 6). At the same time, while adding 15 mol % of CeF_3 or NdF_3 to FLiNaK, the enthalpy values calculated in our model increase to ∼4.4%.

The important segments of the ion mean square displacements are nearly straight lines in every case. The self-diffusion coefficient is determined according to the incline of MSD to time axes. Figure 7 shows the $\langle \Delta r^2 \rangle(t)$ dependences obtained by averaging over 5 initial times t_0 for ions of FLiNaK system containing 15 mol % of CeF_3 at T = 900 K. The largest incline of $\langle \Delta r^2 \rangle(t)$ function to the time axes is for F^- ions, and the least one is for Ce^{3+} ions.

To understand the effect of additives (Ce, Nd) on the kinetic properties of the molten salts, we first calculated the temperature behavior of the self-diffusion coefficients D of ions for pure FLiNaK. Figure 8 shows the calculated dependences $D(T)$, their linear approximation, and the Arrhenius (linear) representation of this dependence obtained from the experiment.[61] We explain the high value of the D coefficient for fluorine ions by their high abundance in the melt. The most

https://doi.org/10.1021/acs.jpcb.2c06915
J. Phys. Chem. B 2023, 127, 1197−1208

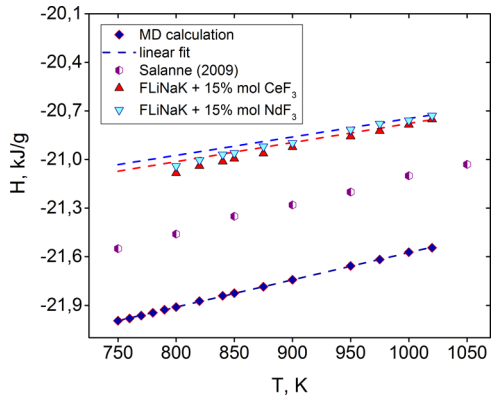

Figure 6. Temperature dependence of the mass enthalpy for FLiNaK (dark-blue rhombus), FLiNaK + 15 mol % CeF_3 (red triangles), and FLiNaK + 15 mol % NdF_3 (blue inverted triangles); dashed lines are the linear fits of the corresponding dependences; half-filled purpura circles show the MD results of work[60] for pure FLiNaK.

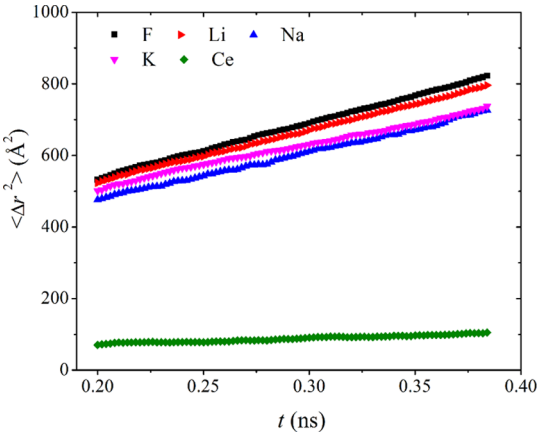

Figure 7. Mean square displacements of FLiNaK + 15 mol % CeF_3 components at T = 900 K.

numerous F^- ions in the FLiNaK eutectic molten salts have significantly more repulsive interactions in the specific ratio than any other ions. Also, in this mixture, there are 2.15 times more F^- ions than the second largest number of Li^+ ions. At the same time, with an equal number of positive and negative ions, the total mass of positive ions in this molten salt is 1.17 times greater than the total mass of F^- ions. The values of the ionic coefficients D obtained from the Arrhenius dependences for the MD calculation and experiment agree within 12−22%. It can be seen from the figure that the $D(T)$ Arrhenius dependencies in the infinite system and that for the MD calculation using PBC are close. In other words, in the entire temperature range under study, the values of the self-diffusion coefficients determined from the approximation dependence $D_\infty(T)$ exceed the corresponding values established from the approximation dependence $D(T)$ by no more than 3%. The results underline that in molten FLiNaK, the mobility of positive ions decreases with their atomic weight. A similar relationship between the mobility of these ions in the molten FLiNaK was obtained in the MD ab initio calculations.[62]

The calculated $D(T)$ and estimated $D_\eta(T)$ dependencies of the self-diffusion coefficients of ions on temperature in the molten salts under consideration are shown in Figure 9. Such dependencies are shown for all types of ions in FLiNaK + 15 mol % CeF_3 and only for Nd^{3+} ions in FLiNaK + 15 mol % NdF_3. The ratio between the D values for the ions included in FLiNaK is identical in both cases. The calculated self-diffusion coefficients decrease from the highest to the lowest as follows: F, Li, Na, K, and Ce. In average, the D values for Ce are lower than that for F by 6 times, and the D coefficient for Nd is 2.6 times lower than that for Ce. Additionally, the integral D coefficient for other ions (F^-, Li^+, Na^+, K^+) in the molten salt with 15 mol % NdF_3 is 7.3% higher compared with the melt containing 15 mol % CeF_3. When passing from the MD system with PBC to the infinite system, a very slight increase (<2%) in the self-diffusion coefficients is observed. It is determined from the approximation $D_\infty(T)$ dependence (relative to that of $D(T)$) for ions included in molten FLiNaK. For heavier ions, Ce^{3+} and Nd^{3+}, the largest increase in D in a similar transition can be 5 and 15%, respectively. Here, the increase in the fraction of the correction is due to the low values of the D coefficient for heavy ions. It follows from ref 47 that electrostatic effects in an ionic system should reduce the D coefficient correction value that transforms the MD system with PBC into an infinite system. The correction varies with system size as $N^{-1/3}$. In the TIP3P water model containing 128 molecules, the correction is estimated at 26%, and for a similar system of 2048 molecules, it is about 9%.[47] Such correction for the self-diffusion coefficients of the FLiNaK components found by us in the model of 20,000 ions does not exceed 3%.

It can be seen that on average, D_η {Nd} value exceeds D_η {Ce} by 1.9 times. At the same time, the integral D_η coefficient for F^-, Li^+, Na^+, and K^+ ions of the molten salts with Ce is 7.0% higher than that for the melts containing Nd. Besides, D_η values for F^-, in average, are lower than that for both Li^+ and Na^+ ions. The D_η values which are inferior to the D values for ions contained in molten FLiNaK indicate that the interaction of these ions more likely corresponds to the interaction of smooth spheres than objects with a rough surface. At the same time, the high D_η values for the Ce^{3+} and Nd^{3+} ions compared to the corresponding D values show that the solvate shells also take part in the motion of these ions.

The temperature dependence of shear viscosity η of the investigated melts in coordinates $\log(\eta)$ $(1000/T)$ is presented in Figure 10. For every system, the experimental and MD data have close values and fit practically on the same straight line. Approximation dependences of MD data for three systems under investigation are

$$\log(\eta) = -1.64626 + 1.99537\cdot(1000/T),\ \text{FLiNaK} \quad (11)$$

$$\log(\eta) = -1.1298 + 1.8252\cdot(1000/T),\ \text{FLiNaK + 15 mol \% } CeF_3 \quad (12)$$

$$\log(\eta) = -0.94608 + 1.68124\cdot(1000/T),\ \text{FLiNaK + 15 mol \% } NdF_3 \quad (13)$$

Figure 10 also demonstrates the experimental data[20] for shear viscosity of pure FLiNaK and the corresponding data obtained in the MD calculation.[60] These data are in good agreement with each other but have some discrepancy with our results. The absence of a description of the FLiNaK preparation and measurement equipment in work[20] creates difficulties in assessing the reliability of the results obtained, presented in the form of an analytical dependence. The data of work[60] differ from the present results because the polarization part of the potential including charge−dipole and dipole−

https://doi.org/10.1021/acs.jpcb.2c06915
J. Phys. Chem. B 2023, 127, 1197−1208

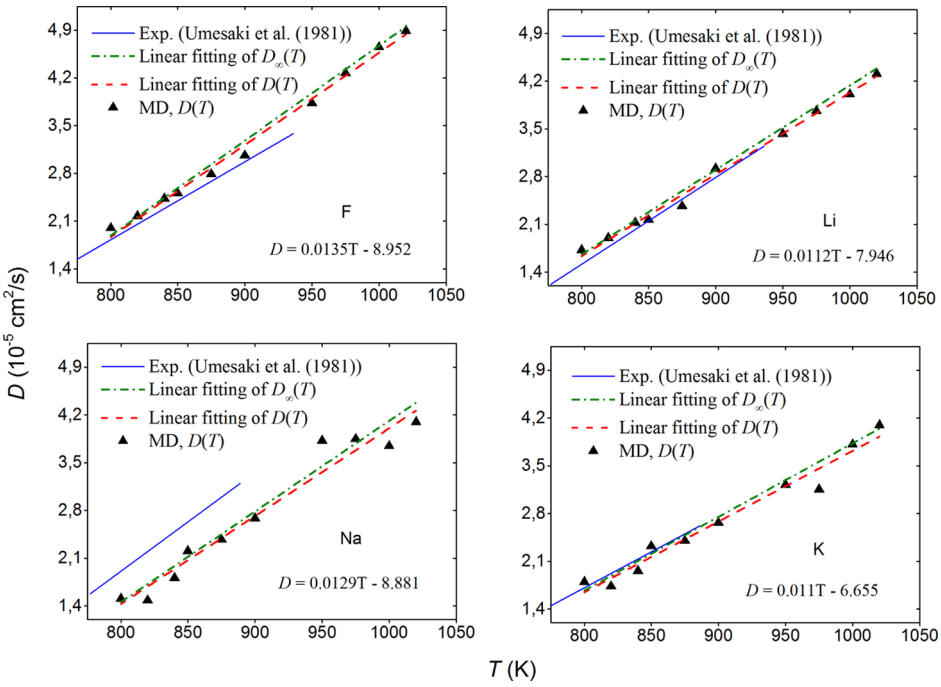

Figure 8. Self-diffusion coefficients of molten FLiNaK components; the linear approximation of the MD calculation is presented as a dotted line and an analytical expression; dashed-dotted lines give a similar approximation of the dependence $D_\infty(T)$; solid lines show the experimental results.[61]

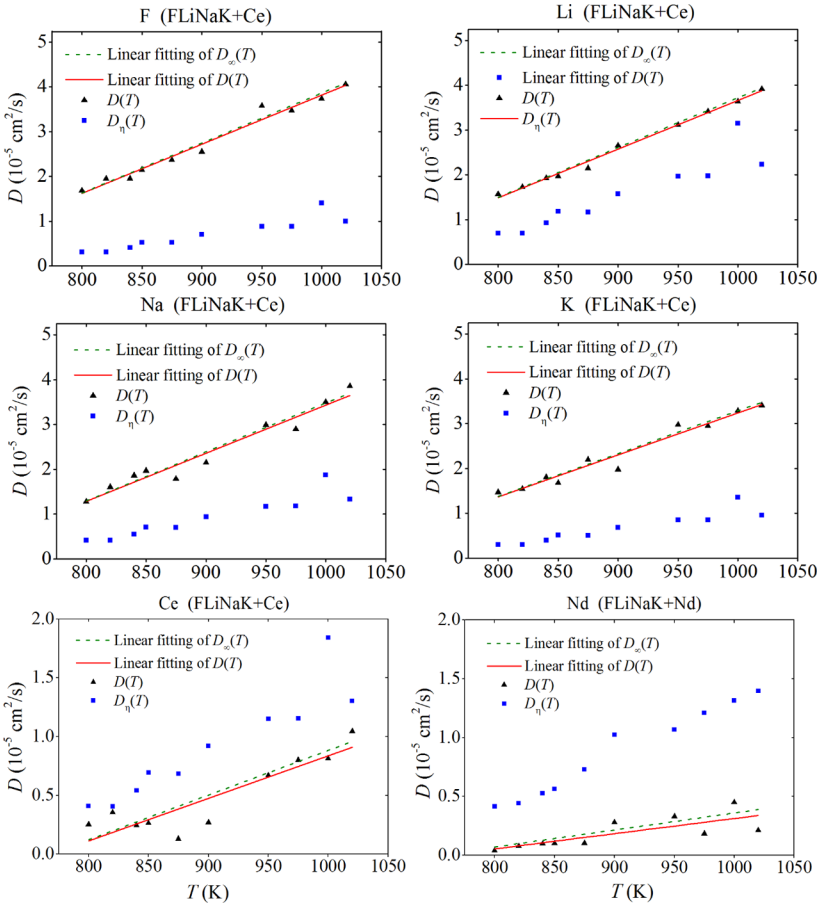

Figure 9. Self-diffusion coefficients D and D_η of ions of the FLiNaK + 15 mol % CeF_3 and FLiNaK + 15 mol % NdF_3 components; solid lines show the linear fit of $D(T)$ dependences; dashed lines give the linear fit of $D_\infty(T)$ dependences.

https://doi.org/10.1021/acs.jpcb.2c06915
J. Phys. Chem. B 2023, 127, 1197−1208

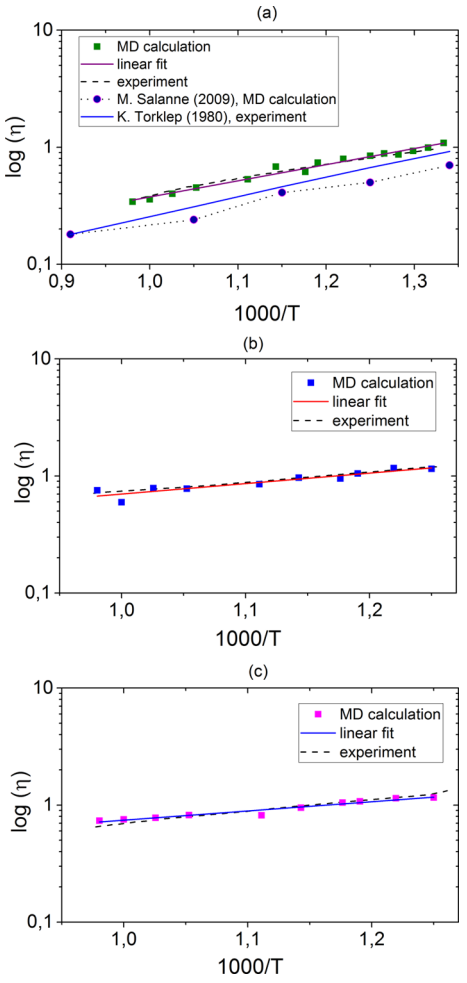

Figure 10. Shear viscosity: (a) molten FLiNaK, (b) FLiNaK + 15 mol % CeF_3, and (c) FLiNaK + 15 mol % NdF_3, obtained in both experiments and MD simulation; the linear approximation of the MD results is also shown as solid lines; dotted and solid lines of (a) represent the simulated[60] and experimental[20] results; shear viscosity is expressed in mPa·s.

dipole terms has been taken into account. In this work, polarization is out of consideration.

The viscosity of the molten salts is closely related to the mobility of the ions. In other words, viscosity determines the movement of individual ions from the initial equilibrium position to a neighboring equilibrium position when the movement occurs in the direction of the fluid flow. The high viscosity of the mixture is mainly created by the slowest moving ions. Strongly coordinated ions form a large inactive shell, thereby increasing the viscosity of the melt. It can be seen from Figure 11 that the more the heavy ions (Ce^{+3} and Nd^{+3}) dissolve in the melts, the higher the viscosity of the melts. The MD calculations show that the viscosity increases linearly with the lanthanide fluoride concentration. These data can be approximated with the linear fit

$$\eta = 2.6661 + 0.2801 \cdot C_i,\ i = CeF_3 \quad (14)$$

$$\eta = 3.1414 + 0.2434 \cdot C_i,\ i = NdF_3 \quad (15)$$

Experimental dependence $\eta(C_i)$ is in good agreement with the simulated results in the case of NdF_3, and they have the discrepancy when CeF_3 dissolves in the melts. Experimental data illustrate that there is an excess viscosity when 3 and 7 mol % CeF_3 dissolve in FLiNaK. However, the excess viscosity disappears, when 15 mol % CeF_3 presents in the melts.

The appearance of the excess viscosity of the melts containing Ce can be explained by the ability of Ce atoms to "adjust" the environment by varying the degree of oxidation between Ce^{4+} and Ce^{3+}. In other words, Ce atom has the ability to tune easily its electronic structure according to the environmental medium "requests". Consequently, at certain conditions, associates can form around Ce atoms.[63] They increase the shear viscosity of the melts. The neodymium lanthanide does not have the ability to vary quickly the degree of oxidation.

The main results obtained in this work can be summarized as follows: for MD calculations, the interatomic potentials describing the interactions between FLiNaK components and additions (CeF_3, NdF_3) are developed. It is shown that the self-diffusion coefficients of ions in molten FLiNaK depend not only on their atomic weights but also on the concentration of the components in the melt. In particular, the high value of the self-diffusion coefficient for F^- ions is due to the high concentration of fluorine in FLiNaK. The insignificance of corrections for the self-diffusion coefficients when converting the results of MD calculations to data for a macroscopic system is proven. The need to correct the Stokes–Einstein formula relating the shear viscosity to the self-diffusion coefficient is demonstrated when applied to the components of molten FLiNaK. The temperature dependences of the self-diffusion coefficients and the shear viscosity of molten FLiNaK + 15 mol % CeF_3 (NdF_3) systems have been studied. The concentration

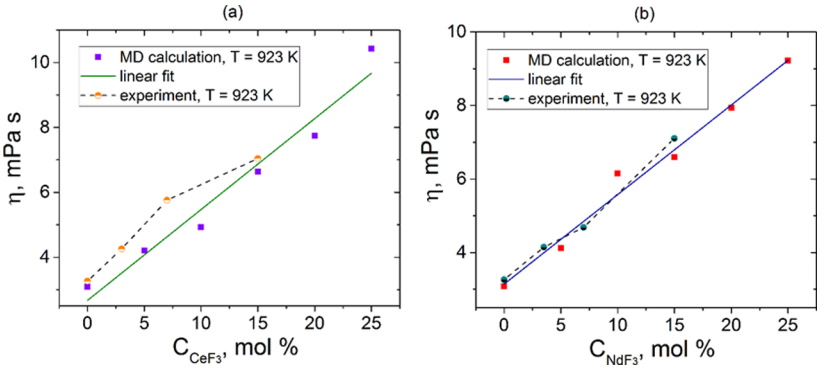

Figure 11. Comparison of the MD calculation results and experimental data of the shear viscosity concentration dependence for systems (a) FLiNaK + (mol %) CeF_3 and (b) FLiNaK + (mol %) NdF_3; solid lines show the linear fit of our MD results.

https://doi.org/10.1021/acs.jpcb.2c06915
J. Phys. Chem. B 2023, 127, 1197−1208

dependences of the viscosity of these systems are studied experimentally and by the MD simulation method.

CONCLUSIONS

The behavior of the shear viscosity and self-diffusion coefficients in the advanced molten FLiNaK with lanthanide fluorides (CeF_3 and NdF_3) dissolved in it intended for use in MSR is studied experimentally and by MD calculations over a wide temperature range. Good agreement has been achieved between the temperature dependences of the calculated and experimental self-diffusion coefficients and shear viscosity. However, acceptable agreement between the concentration dependences for the shear viscosity is obtained only in the case of the presence of NdF_3 in this molten salt. The experimental dependence of the viscosity on the CeF_3 content in FLiNaK deviates noticeably from the corresponding dependence of the MD calculations.

Thus, the important kinetic properties of the molten FLiNaK with CeF_3 and NdF_3 dissolved in it have been studied in detail in a computer model. In the future, this model successfully validated according to the experimental data could be used for the prediction of the behavior of the kinetic coefficients of such complicated for experiment systems as FLiNaK with additions of minor actinide fluorides (PuF_3, AmF_3).

ASSOCIATED CONTENT

Supporting Information

The Supporting Information is available free of charge at https://pubs.acs.org/doi/10.1021/acs.jpcb.2c06915.

Born−Huggins−Mayer potential for FLiNaK (PDF)

AUTHOR INFORMATION

Corresponding Author

A. Y. Galashev − *Institute of High-Temperature Electrochemistry, Ural Branch of Russian Academy of Sciences, Yekaterinburg 620990, Russia;* orcid.org/0000-0002-2705-1946; Email: galashev@ihte.uran.ru

Authors

O. R. Rakhmanova − *Institute of High-Temperature Electrochemistry, Ural Branch of Russian Academy of Sciences, Yekaterinburg 620990, Russia*

K. A. Abramova − *Institute of High-Temperature Electrochemistry, Ural Branch of Russian Academy of Sciences, Yekaterinburg 620990, Russia;* orcid.org/0000-0001-6521-1966

K. P. Katin − *National Research Nuclear University MIPhI, Moscow 115409, Russia;* orcid.org/0000-0003-0225-5712

M. M. Maslov − *National Research Nuclear University MIPhI, Moscow 115409, Russia;* orcid.org/0000-0001-8498-4817

O. Y. Tkacheva − *Institute of High-Temperature Electrochemistry, Ural Branch of Russian Academy of Sciences, Yekaterinburg 620990, Russia*

A. V. Rudenko − *Institute of High-Temperature Electrochemistry, Ural Branch of Russian Academy of Sciences, Yekaterinburg 620990, Russia*

A. A. Kataev − *Institute of High-Temperature Electrochemistry, Ural Branch of Russian Academy of Sciences, Yekaterinburg 620990, Russia*

Y. P. Zaikov − *Institute of High-Temperature Electrochemistry, Ural Branch of Russian Academy of Sciences, Yekaterinburg 620990, Russia*

Complete contact information is available at: https://pubs.acs.org/10.1021/acs.jpcb.2c06915

Notes

The authors declare no competing financial interest.

ACKNOWLEDGMENTS

This work was executed in the frame of the scientific theme of Institute of High-Temperature Electrochemistry UB RAS, no FUME-2022-0005, registration no 122020100205-5.

REFERENCES

(1) Adamov, E. O.; Dzhalavyan, A. V.; Lopatkin, A. V.; Molokanov, N. A.; Muravyov, E. V.; Orlov, V. V.; Kal'akin, S. G.; Rachkov, V. I.; Troyanov, V. M.; Avrorin, E. N.; et al. Conceptual Framework of a Strategy for the Development of Nuclear Power in Russia to 2100. *Atom. Energy* **2012**, *112*, 391−403.

(2) Biss, K. H.; Thomauske, B. Shortening Transmutation Time by Using the Molten Salt Reactor. *Ann. Nucl. Energy* **2015**, *83*, 25−33.

(3) Ponomarev, L. I.; Seregin, M. B.; Parshin, A. P.; Mel'nikov, S. A.; Mikhalichenko, A. A.; Zagorets, L. P.; Manuilov, R. N.; Rzheutskii, A. A. Fuel Salt for the Molten-Salt Reactor. *Atom. Energy* **2013**, *115*, 5−10.

(4) Magnusson, J.; Memmott, M.; Munro, T. Review of Thermophysical Property Methods Applied to Fueled and Un-Fueled Molten Salts. *Ann. Nucl. Energy* **2020**, *146*, 107608.

(5) Beneš, O.; Konings, R. J. M. Thermodynamic Properties and Phase Diagrams of Fluoride Salts for Nuclear Applications. *J. Fluorine Chem.* **2009**, *130*, 22−29.

(6) Robertson, S. G.; Short, M. P. Design and Performance of a Molten Fluoride Salt-Compatible Optical Thermophysical Property Measurement System. *Rev. Sci. Instrum.* **2021**, *92*, 064905.

(7) Williams, D. F.; Britt, P. F.*Molten Salt Chemistry Workshop: Report for the US Department of Energy*, Technical report; Oak Ridge National Laboratory: Oak Ridge, TN, USA; 2017.

(8) Boyd, S.; Taylor, C.*Molten Salt Reactors and Thorium Energy*; Dolan, T. J., Ed.; Woodhead Publishing: Cambridge, MA, USA, 2017; pp 30−45.

(9) Bahri, C. N. A. C. Z.; Al-Areqi, W. M.; Ruf, M. I. F. M.; Majid, A. A. Characteristic of Molten Fluoride Salt System LiF-BeF_2 (Flibe) and LiF-NaF-KF (Flinak) as Coolant and Fuel Carrier in Molten Salt Reactor (MSR). *AIP Conf. Proc.* **2017**, *1799*, 040008.

(10) Forsberg, C. W.; Peterson, P. F.; Zhao, H. High-Temperature Liquid Fluoride-Salt Closed-Brayton Cycle Solar Power Towers. *J. Sol. Energy Eng.* **2007**, *129*, 141−146.

(11) Frandsen, D. A.; Nickerson, S. D.; Clark, A. D.; Solano, E.; Baral, R.; Williams, J.; Neuefeind, J.; Memmott, M. The Structure of Molten FLiNaK. *J. Nucl. Mater.* **2020**, *537*, 152219.

(12) Kenisarin, M. M. High-Temperature Phase Change Materials for Thermal Energy Storage. *Renewable Sustainable Energy Rev.* **2010**, *14*, 955−970.

(13) Romatoski, R. R.; Hu, L. W. Fluoride Salt Coolant Properties for Nuclear Reactor Applications: A Review. *Ann. Nucl. Energy* **2017**, *109*, 635−647.

(14) Schreuder, M.; Ocádiz Flores, J.; Gheribi, A.; Beneš, O.; Griveau, J.-C.; Colineau, E.; Konings, R. J. M.; Smith, A. L. Experimental and Computational Exploration of the NaF−ThF_4 Fuel System: Structure and Thermochemistry. *J. Phys. Chem. B* **2021**, *125*, 8558−8571.

(15) Lynch, T.; Birkner, N.; Christian, M.; Wrubel, J.; Schorne-Pinto, J.; Van Veelen, A.; Bargar, J.; Besmann, T.; Brinkman, K.; Chiu, W. In situ determination of speciation and local structure of NaCl−$SrCl_2$ and LiF−ZrF_4 molten salts. *J. Phys. Chem. B* **2022**, *126*, 1539−1550.

(16) Clark, A.; Lee, W.; Solano, A.; Williams, T.; Meyer, T.; Tait, G.; Battraw, G.; Nickerson, B.; Nickerson, S. Complexation of Mo in FLiNaK Molten Salt: Insight from Ab initio Molecular Dynamics. *J. Phys. Chem. B* **2021**, *125*, 211−218.
(17) Ponomarev, L. I.; Seregin, M. V.; Michalichenko, A. A.; Parshin, A. P.; Zagorez, L. P. Validation of Actinide Simulators for Studying Solubility in Fuel Salt of Molten-Salt Reactor. *Atom. Energy* **2012**, *112*, 417−422.
(18) Lizin, A. A.; Tomilin, S. V.; Gnevashov, O. E.; Gazizov, R. K.; Osipenko, A. G.; Kormilitsyn, M. V.; Baranov, A. A.; Zaharova, L. V.; Naumov, V. S.; Ponomarev, L. I. PuF_3, AmF_3, CeF_3, NdF_3 Solubility in LiF-NaF-KF Melt. *Atom. Energy* **2013**, *115*, 11−17.
(19) Serrano-López, R.; Fradera, J.; Cuesta-López, S. Molten Salts Database for Energy Applications. *Chem. Eng. Process.* **2013**, *73*, 87−102.
(20) Toerklep, K.; Oeye, H. A. Viscosity of the Eutectic Lithium Fluoride-Sodium Fluoride-Potassium Fluoride Melt (FLINAK). *J. Chem. Eng. Data* **1980**, *25*, 16−17.
(21) Kubíková, B.; Pavlík, V.; Macková, I.; Boča, M. Surface Tension and Viscosity of the Molten $(LiF−NaF−KF)_{eut}−K_2ZrF_6$ System. *Monatsh. Chem.* **2012**, *143*, 1459−1462.
(22) Cibulková, J.; Chrenková, M.; Vasiljev, R.; Kremenetsky, V.; Boča, M. Density and Viscosity of the $(LiF + NaF + KF)_{eut}$ (1) + K_2TaF_7 (2) + Ta_2O_5 (3) Melts. *J. Chem. Eng. Data* **2006**, *51*, 984−987.
(23) Chrenková, M.; Daněk, V.; Silný, R.; Kremenetsky, F.; Polyakov, V.; Polyakov, E. Density and Viscosity of the $(LiF-NaF-KF)_{eut}$-KBF_4-B_2O_3 Melts. *J. Mol. Liq.* **2003**, *102*, 213−226.
(24) Tasidou, K. A.; Magnusson, J.; Munro, T.; Assael, M. J. Reference Correlations for the Viscosity of Molten LiF−NaF−KF, LiF−BeF_2, and $Li_2CO_3−Na_2CO_3−K_2CO_3$. *J. Phys. Chem. Ref. Data* **2019**, *48*, 043102.
(25) Merzlyakov, A.; Ignatiev, V.; Abalin, S. Viscosity of LiF−NaF−KF Eutectic and Effect of Cerium Trifluoride and Uranium Tetrafluoride Additions. *Nucl. Eng. Des.* **2014**, *278*, 268−273.
(26) An, X.-H.; Cheng, J.-H.; Yin, H.-Q.; Xie, L.-D. P.; Zhang, P. Thermal Conductivity of High Temperature Fluoride Molten Salt Determined by Laser Flash Technique. *Int. J. Heat Mass Transfer* **2015**, *90*, 872−877.
(27) Adams, D. J.; McDonald, I. R. Rigid-Ion Models of the Interionic Potential in the Alkali Halides. *J. Phys. C: Solid State Phys.* **1974**, *7*, 2761−2775.
(28) Giannozzi, P.; Baroni, S.; Bonini, N.; Calandra, M.; Car, R.; Cavazzoni, C.; Ceresoli, D.; Chiarotti, G.; Cococcioni, M.; Dabo, I.; Dal Corso, A.; de Gironcoli, S.; Fabris, S.; Fratesi, G.; Gebauer, R.; Gerstmann, U.; Gougoussis, C.; Kokalj, A.; Lazzeri, M.; Martin-Samos, L.; Marzari, N.; Mauri, F.; Mazzarello, R.; Paolini, S.; Pasquarello, A.; Paulatto, L.; Sbraccia, C.; Scandolo, S.; Sclauzero, G.; Seitsonen, A. P.; Smogunov, A.; Umari, P.; Wentzcovitch, R. M. QUANTUM ESPRESSO: A Modular and Open-Source Software Project for Quantum Simulations of Materials. *J. Phys.: Condens. Matter* **2009**, *21*, 395502.
(29) Giannozzi, P.; Andreussi, O.; Brumme, T.; Bunau, O.; Buongiorno Nardelli, M.; Calandra, M.; Car, R.; Cavazzoni, C.; Ceresoli, D.; Cococcioni, M.; et al. Advanced Capabilities for Materials Modelling with Quantum ESPRESSO. *J. Phys.: Condens. Matter* **2017**, *29*, 465901.
(30) Blöchl, P. E. Projector Augmented-Wave Method. *Phys. Rev. B: Condens. Matter Mater. Phys.* **1994**, *50*, 17953−17979.
(31) Kresse, G.; Joubert, D. From Ultrasoft Pseudopotentials to the Projector Augmented-Wave Method. *Phys. Rev. B: Condens. Matter Mater. Phys.* **1999**, *59*, 1758−1775.
(32) Grimme, S. Semiempirical GGA-type Density Functional Constructed with a Long-Range Dispersion Correction. *J. Comput. Chem.* **2006**, *27*, 1787−1799.
(33) Cui, R.; Wang, C. In situ High Temperature Raman and DFT Analysis of Cerium Fluoride and Oxyfluoride Structures in Molten FLiNaK. *J. Raman Spectrosc.* **2021**, *52*, 1148−1154.
(34) Prencipe, M.; Zupan, A.; Dovesi, R.; Aprà, E.; Saunders, V. R. Ab initio Study of the Structural Properties of LiF, NaF, KF, LiCl, NaCl, and KCl. *Phys. Rev. B: Condens. Matter Mater. Phys.* **1995**, *51*, 3391−3396.
(35) Melchionna, S.; Ciccotti, G.; Lee Holian, B. L. Hoover NPT Dynamics for Systems Varying in Size and Shape. *Mol. Phys.* **1993**, *78*, 533−544.
(36) Martyna, G. J.; Tobias, D. J.; Klein, M. L. Constant Pressure Molecular Dynamics Algorithms. *J. Chem. Phys.* **1994**, *101*, 4177−4189.
(37) Hockney, R. W.; Eastwood, J. W.*Computer Simulation Using Particles*; Adam Hilger: Bristol, U.K., 1988.
(38) Darden, T.; York, D.; Pedersen, L. Particle Mesh Ewald: An N·log(N) Method for Ewald Sums in Large Systems. *J. Chem. Phys.* **1993**, *98*, 10089.
(39) Pollock, E. L.; Glosli, J. Comments on P^3M, FMM, and the Ewald Method for Large Periodic Coulombic Systems. *Comput. Phys. Commun.* **1996**, *95*, 93−110.
(40) Allen, M. P.; Tlldesley, D. J.*Computer Simulation of Liquids*; Oxford University Press: New York, USA, 1987.
(41) Korczak, W.; Mikołajczak, P. Crystal Growth and Temperature Variation of the Lattice Parameters in LaF_3, CeF_3, PrF_3 and NdF_3. *J. Cryst. Growth* **1983**, *61*, 601−605.
(42) Rogers, D. J.; Yoko, T.; Janz, G. J. Fusion Properties and Heat Capacities of the Eutectic Lithium Fluoride-Sodium Fluoride-Potassium Fluoride Melt. *J. Chem. Eng. Data* **1982**, *27*, 366−367.
(43) Mushnikov, P. N.; Tkacheva, O. Yu.; Kholkina, A. S.; Zaikov, Yu. P.; Shishkin, V. Yu.; Dub, A. V. Phase Diagram of the Quasibinary System LiF−NaF−KF−CeF_3. *Atom. Energy* **2022**, *131*, 263−267.
(44) Kim, C. M.; Yoon, S. P.; Cho, S. K. Determination of Diffusion Coefficient in High Temperature Molten Salt Using Cyclic Voltammetry on Microwire Electrode: Its Validity and Limitation. *J. Electroanal. Chem.* **2021**, *894*, 115353.
(45) Song, Y.; Jiang, B.; Li, F. L. Molecular Dynamic Simulations of Selective Self-diffusion of $CH_4/CO_2/H2O/N_2$ in Coal. *IOP Conf. Ser.: Mater. Sci. Eng.* **2017**, *213*, 012014.
(46) Errington, J. R.; Debenedetti, P. G. Relationship Between Structural Order and the Anomalies of Liquid Water. *Nature* **2001**, *409*, 318−321.
(47) Yeh, I.-C.; Hummer, G. System-Size Dependence of Diffusion Coefficients and Viscosities from Molecular Dynamics Simulations with Periodic Boundary Conditions. *J. Phys. Chem. B* **2004**, *108*, 15873−15879.
(48) Nijboer, B. R. A.; Ruijgrok, T. W. On the Energy per Particle in Three- and Two-Dimensional Wigner Lattices. *J. Stat. Phys.* **1988**, *53*, 361−382.
(49) Armstrong, J. A.; Ballone, P. Computational Verification of Two Universal Relations for Simple Ionic Liquids. Kinetic Properties of a Model 2:1 Molten Salt. *J. Phys. Chem. B* **2011**, *115*, 4927−4938.
(50) Galamba, N.; Nieto de Castro, C. N.; Ely, J. F. Shear Viscosity of Molten Alkali Halides from Equilibrium and None Equilibrium Molecular-Dynamics Simulations. *J. Chem. Phys.* **2005**, *122*, 224501.
(51) Wang, J.; Wu, J.; Sun, Z.; Lu, G.; Yu, J. Molecular dynamics study of the transport properties and local structures of molten binary systems (Li, Na)Cl, (Li, K)Cl and (Na, K)Cl. *J. Mol. Liq.* **2015**, *209*, 498−507.
(52) Plimpton, S. Fast Parallel Algorithms for Short-Range Molecular Dynamics. *J. Comp. Physiol.* **1995**, *117*, 1.
(53) Mushnikov, P.; Tkacheva, O.; Voronin, V.; Shishkin, V.; Zaikov, Y. Investigation of the Quasi-Binary Phase Diagram FLiNaK-NdF_3. *Materials* **2021**, *14*, 6428−6434.
(54) Rudenko, A.; Kataev, A.; Tkacheva, O. Dynamic Viscosity of the NaF-KF-NdF_3 Molten System. *Materials* **2022**, *15*, 4884−4895.
(55) Zakiryanov, D. O. Applying the Born-Mayer Model to Describe the Physicochemical Properties of FLiNaK Ternary Melt. *Compd. Theory Chem.* **2023**, *1219*, 113951.
(56) Nam, H. O.; Bengtson, A.; Vörtler, K.; Saha, S.; Sakidja, R.; Morgan, D. First-Principles Molecular Dynamics Modeling of the

https://doi.org/10.1021/acs.jpcb.2c06915
J. Phys. Chem. B 2023, 127, 1197−1208

Molten Fluoride Salt with Cr Solute. *J. Nucl. Mater.* **2014**, *449*, 148−157.
(57) Gallagher, R. C.; Birri, A.; Russell, N. G.; Phan, A.-T.; Gheribi, A. E. Investigation of the Thermal Conductivity of Molten LiF-NaF-KF with Experiments, Theory, and Equilibrium Molecular Dynamics. *J. Mol. Liq.* **2022**, *361*, 119151.
(58) Ludwig, R. The Effect of Dispersion Forces on the Interaction Energies and Far Infrared Spectra of Protic Ionic Liquids. *Phys. Chem. Chem. Phys.* **2015**, *17*, 13790−13793.
(59) Gallagher, R. C.; Agca, C.; Russell, N.; McMurray, J. W.; Bull Ezell, N. D. Assessment of Molten Eutectic LiF-NaF-KF Density through Experimental Determination and Semiempirical Modeling. *J. Chem. Eng. Data* **2022**, *67*, 1406−1414.
(60) Salanne, M.; Simon, C.; Turq, P.; Madden, P. A. Heat-Transport Properties of Molten Fluorides: Determination from First-Principle. *J. Fluorine Chem.* **2009**, *130*, 38−44.
(61) Umesaki, N.; Iwamoto, N.; Tsunawaki, Y.; Ohno, H. K.; Furukawa, K. Self-diffusion of Lithium, Sodium, Potassium and Fluorine in a Molten LiF+NaF+KF Eutectic Mixture. *J. Chem. Soc., Faraday Trans. 1* **1981**, *77*, 169−175.
(62) Mignacca, B.; Locatelli, G. Economics and Finance of Molten Salt Reactors. *Prog. Nucl. Energy* **2020**, *129*, 103503.
(63) Xu, C.; Qu, X. Cerium Oxide Nanoparticle: A Remarkably Versatile Rare Earth Nanomaterial for Biological Applications. *NPG Asia Mater.* **2014**, *6*, No. e90.

https://doi.org/10.1021/acs.jpcb.2c06915
J. Phys. Chem. B 2023, 127, 1197−1208